Synthesis of High Quality Single-Walled Carbon Nanotube Silks by the Arc Discharge Technique

Hong-wei Zhu,* Bin Jiang, Cai-lu Xu, and De-hai Wu

Department of Mechanical Engineering, Tsinghua University, Beijing 100084, P. R. China

Received: November 19, 2002; In Final Form: March 13, 2003

We have modified the conventional arc discharge method for the synthesis of high quality single-walled carbon nanotube (SWNT) silks with high purity (over 70%) by using a hollow cathode that can collect SWNTs effectively. Characterizations of these SWNT materials by XRD, UV−vis−near-IR, Raman were taken. Finally a simple process involving subsequent acid treatment to align the SWNTs locally in the thin silks was introduced.

1. Introduction

In the conventional arc synthesis of single-walled carbon nanotubes (SWNTs),[1] a rod-like graphite cathode was used to collect SWNTs: (a) web soot, hung between the chamber wall and the cathode; (b) rubbery film, condensed on the chamber wall; (c) collar, around the cathode end. Both products (a) and (b) had low purity and density since the reaction in the arc discharge plasma region was very complicated. High-quality SWNTs could only be found in the collar around the cathode with densest morphology and a high purity of ∼70%.[1] It was believed that the cathode shape had an important influence on the morphology and quality of SWNT products. Recently, a bowl-shaped cathode was used to produce super SWNT bundles,[2] and the difference between these materials and previously prepared SWNTs was only the macroscopic state; microstructure and purity were still similar to SWNT soot based on their TEM measurements. Huczko et al. have reported the generation of aligned carbon nanofibers by using a hollow graphite cathode discharge CVD technique.[3]

Stimulated by this idea, we used thick hollow graphite as cathode in the arc discharge process to prepare silk-like SWNT materials with the same quality of the SWNT collar. After optimizing the operating conditions and the composition of the catalyst, silk-like films of SWNTs with controllable thickness (up to 1 mm) were grown in abundance on the inner surface of the cathode. The SWNT silks could be torn into thinner films with semitransparent view, and a tearing sound could be heard just like paper cracking. Carbon nanotubes in the macroscopic state, such as SWNT fibers and ribbons,[4] long SWNT ropes from hydrogen arc discharge method,[5] and 20 cm long SWNT strands,[6] have been reported. Our SWNT silks can also be identified as a free-standing macroscopic morphology. Direct measurements can be carried out on the as-grown materials without any further posttreatment. A simple chemical treatment involving immersion in sulfuric acid and nitric acid can be used to align SWNTs locally in the silks.

2. Experimental Section

In our experiment, a conventional arc discharge device was used with a hollow graphite cathode (2 cm i.d.). The buffer gas was pure helium (>99.999%). Figure 1A shows a schematic drawing of the arrangement of the electrodes. The anode was a cylindric graphite rod (Φ6 mm, 100 mm long) in which a hole (Φ3 mm) had been drilled and filled with 4.2 at. % Ni, l at. % Y (or l at. % Ce), and 0.8 at. % FeS. Cerium was found to be a good element for stabilizing the electric arc, though the SWNT products as-grown from Ce had a low purity.

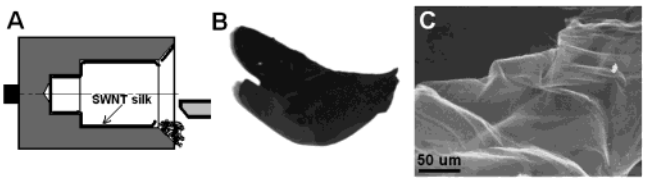

Figure 1. Schematic diagram of the hollow cathode (A), the optical photo (B), and low resolution SEM image (C) of as-grown SWNT silk.

In the arc process, in addition to the conventional SWNT products mentioned above, silk-like materials with smooth, shiny surfaces and uniform thickness were found abundantly on the inner wall of the hollow cathode (as the arrow indicated in Figure 1A). The silks became denser and thicker around 800 mbar (Figure 1B); the current was maintained at 50 A during synthesis to gain high quality products. When the depth of hole in the cathode was up to 2.5 cm, we got good and free-standing silk-like materials which allowed us to directly measure their macroscopic properties (such as XRD, UV−vis−NIR). Such a cathode provided a substrate for the growing SWNTs, which allowed the catalysts to be supplied in a more controllable way. The silk-like materials were identified as high-quality SWNT films with layered structure (see Figure 2a) by using scanning electron microscopy (SEM), transmission electron microscopy (TEM), and Raman scattering spectroscopy. The silken and smooth surfaces can be seen clearly (Figure 1C).

3. Results and Discussion

When the arc time was increased, the thickness of SWNT silk increased with a growth rate of up to ∼0.5 mm/min. Typical synthesis times were 2 min to avoid sintering of the silks under high temperature. Figure 2b−e shows the SEM and TEM images of the SWNT silks at different resolutions. As shown in Figure 2b, high-density SWNT bundles were observed at random orientation with a few nanoparticles and amorphous carbon. Figure 2c shows a part of the thinnest area, showing a web-like

* Corresponding author. Phone: +86-10-62783798; Fax: +86-10-62782413; E-mail: zhuhongwei98@mails.tsinghua.edu.cn.

10.1021/jp027490x CCC: $25.00
Published on Web 06/17/2003

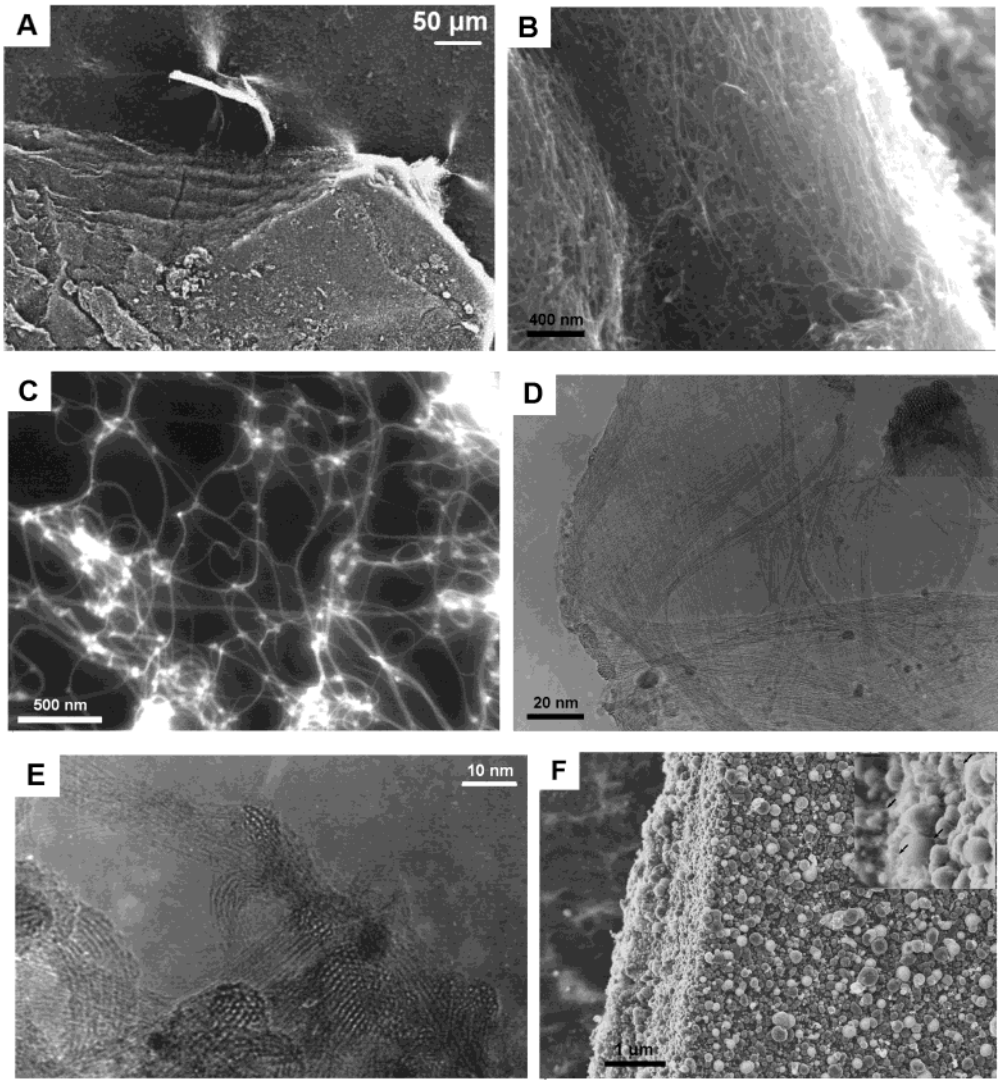

Figure 2. (A) Layered structure of the SWNT silks; (B) SEM image of the thickest area, similar to the "buckypaper";[8] (C) SEM image of the thinnest area; (D) TEM image of the thin SWNT film; (E) high-resolution TEM image showing cross section of the edge of the SWNT film; (F) SEM image of the first layer deposited on the inner-wall of the graphite, rich of metal nanoparticles. The SWNT materials were examined using SEM (Hitachi S-900) and TEM (JEOL, JEM-200CX) operated at 200 kV.

structure formed by entangled SWNT bundles with diameters of 20∼50 nm. For TEM observation, a piece of SWNT silk was selected and torn by tweezers and affixed on the TEM grid by wetting with a drop of ethanol or acetone. Thus it is free of ultrasonic dispersion, no destroying the original structure (the alignment and interrelationships) before observation.

It can be seen that the SWNT bundles in silks have a very narrow distribution of diameters (1.2∼1.4 nm). Every layer of the SWNT silk consists of crossing ordered bundles, which display a polycrystalline organization (Figure 2d), and are also further affirmed by XRD measurements (Figure 3). Many lift-up tips of SWNT bundles can be seen in a closer view (Figure 2e).

The XRD experiments were carried out directly on a piece of SWNT silk with an area of ∼1 cm × 2 cm. In XRD profiles of as-grown materials (Figure 3), the first diffraction peak is found at about 0.45 $Å^{-1}$, a typical value which corresponds to the (1,0) peak of the SWNT bundles.[7,8] For SWNT silks, the nanotubes form a two-dimensional (2D) hexagonal array perpendicular to the bundle axis, with the hexagonal parameter $a = 1.6$ nm for SWNT diameters around 1.3 nm. A weak peak around 0.73 $Å^{-1}$ that corresponds to the (1,1) peak of the SWNT bundles is visible for SWNT collar and silk. Higher order diffraction peaks at Q∼1.17 and 1.55 $Å^{-1}$, which correspond to the (2,1) and to the (2,2) and to the (3,1) peaks of the SWNT bundles, are also clearly visible for SWNT silk. These dense peaks from as-grown materials without any posttreatments indicated that our SWNT silks have high purity and density which is similar to SWNT collar.[1] In addition, assignment of the diffraction peaks above 1.7 $Å^{-1}$ shows the presence of graphitic nanoparticles (1.82 $Å^{-1}$) and residual graphite (1.87 $Å^{-1}$) in the silk.

EDX analysis indicated that there was only a low content of metal particles left in the thin silks but they are distributed in other SWNT products, especially in SWNT soot. We believed that such a hollow cathode certainly provided a substrate for the formation of carbon-film nanostructures. At the beginning of the arc process (3∼6 s) the arc was unstable, thus the substrate was generated. Figure 2f is a typical TEM image of the substrate surface, a high content of metal catalysts with a relatively wider distribution of diameters was present in the surface layer with a typical thickness of 2 μm. SWNT thin silks may also involve a three-step growth process: SWNT seed generation, catalysts deposit, and thin film growth,[2] which was similar to SWNT growth in the conventional arc discharge. The only difference was that most of the catalyst particles were deposited first on

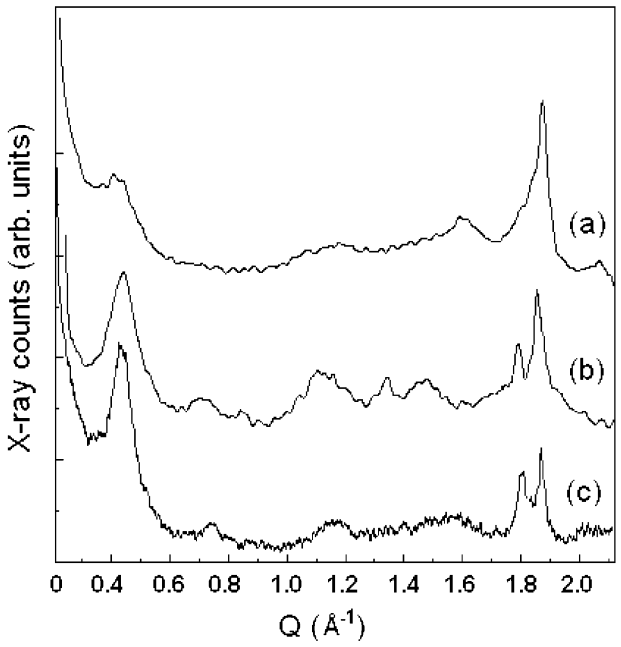

Figure 3. XRD profiles of (A) SWNT soot, (B) SWNT collar, and (C) SWNT silk. X-ray experiments were performed using a rotating copper anode generator. The Cu Kα wavelength ($\lambda = 1.5418$ Å) was selected using a doubly bent graphite monochromator.

the inner surface of the hollow cathode. The hollow cathode can direct the carbon species along the temperature gradient to form the SWNTs. The inset of Figure 2f shows some small diameter bundles (~10 nm) protruding from these particles. Once the SWNT silks are formed, they build a substrate for subsequent deposit.

The optical properties of SWNT silks were also measured directly. Figure 4a presents a typical Raman spectrum (excited by 514 nm laser) of the thin silks prepared with the Ni/Y/FeS catalysts at a pressure of 800 mbar. This spectrum confirms that the silk contains SWNTs, as evidenced by the characteristic SWNT peaks, i.e., the shoulder peak around l567 cm^{-1} and the radical breathing peak 184 cm^{-1}. The many breathing-mode peaks indicate a narrow distribution of SWNT diameters, which is consistent with the high-resolution TEM observations. According to the relation of the diameter and Raman shift, the RBM frequency of 184 cm^{-1} corresponds to SWNTs with diameters of l.3 nm. Also, a 633 nm laser was used to check the metallic component in the SWNT silks, showing the SWNT properties (broad and asymmetric Breit−Wigner−Fano line shape around 1591 cm^{-1} [9]) and narrow diameter distribution (Figure 4b). For comparison, a Raman spectrum from SWNT soot is also presented in Figure 4c, excited by a 633 nm laser, while a clear downward shift of the G peak to 1582 cm^{-1} can be seen clearly, showing the rich present of the impurities of amorphous carbon and metal nanoparticles, the heating effect moving the G mode downward to low frequency when the surface temperature increased.[10] Based on this idea, a qualitative and quantitative analysis method using Raman spectra could be developed to estimate the purity of the SWNT materials.

In the direct UV−vis−NIR measurements, neither the spraying process[9] nor sonication in organic solution[11] was needed. We prepared the sample for measurement by adhering a piece of semitransparent very thin silk on the Si wafer directly, wetting by ethanol, then drying naturally. UV−vis−NIR spectra can provide evidence for the relation between the 1D nature of the energy bands and the van Hove singularities.[11] As shown in Figure 4b, the broad peak centered at 1600 nm is due to the first van Hove singularity in semiconducting nanotubes with bundle form, while the second van Hove singularity is seen centered at 900 nm. A third set of peaks centered near 600 nm is assigned to the first van Hove transition of metallic SWNTs. This information further shows the intrinsic high purity of our SWNT silks because only purified and annealed samples showed dense van Hove peaks based on the previous report[11] and our experimental result on SWNT soot.

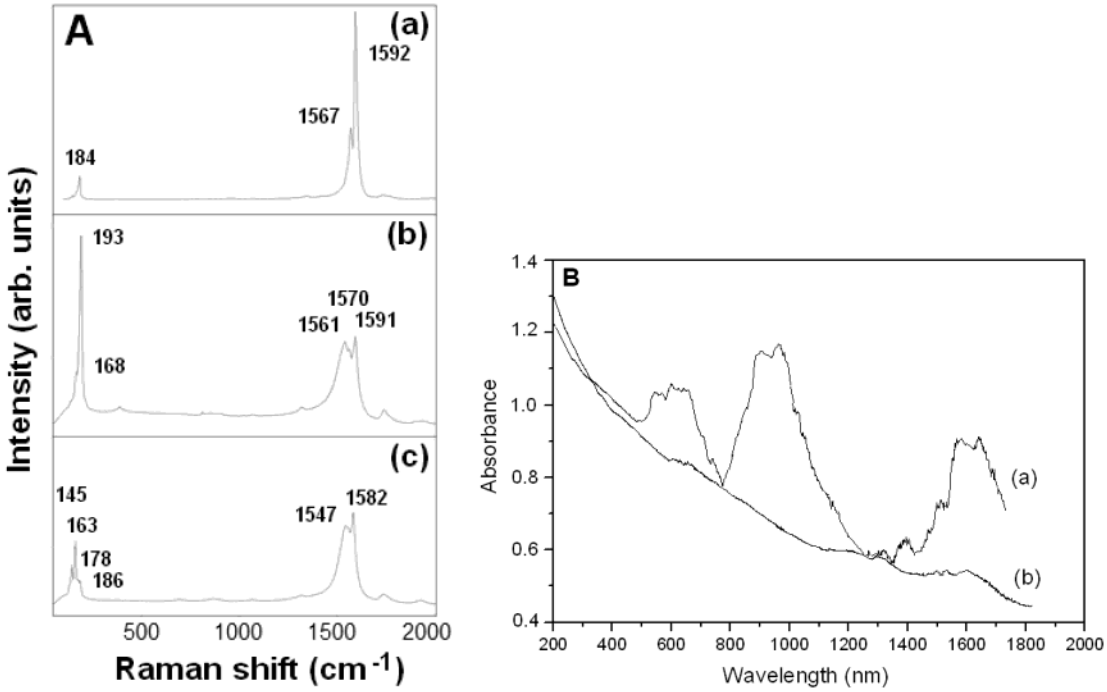

Figure 4. Optical properties measurements. (A) Raman spectra were excited with the 633 nm of (He/Ne laser) and 514 nm (Ar^+ laser) lines in the backscattering configuration with a micro-Raman spectrometer (Renishaw 2000) fitted with a 50× objective. (B) Direct UV−vis−NIR measurements on SWNT silks (a), compare with the result of soot suspension in benzene dichloride (b). UV−vis−NIR spectra were obtained with Shimadzu UV-3100 PC spectrometer.

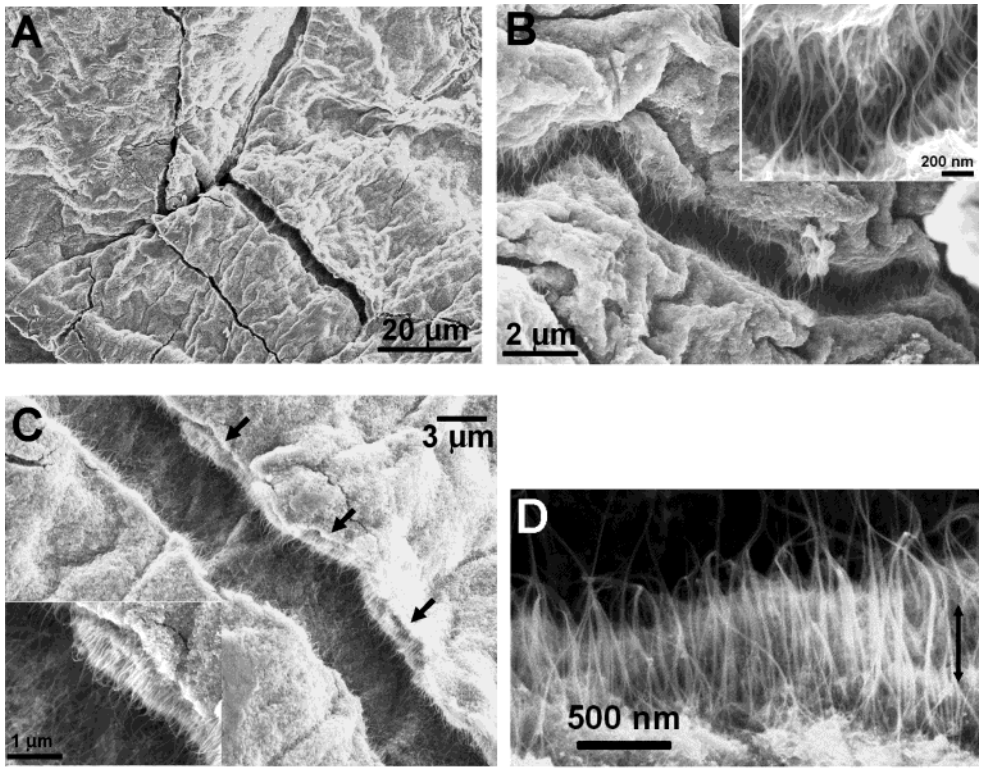

Figure 5. A simple method to align SWNTs. (A) Surface of SWNT thick film after simple acid treatments, scale bar 20 μm. (B) After 2 M H_2SO_4 treatment, scale bar 2 μm. Inset: The parallel SWNT bundles are clearly seen, scale bar 200 nm. (C) After double-acid treatment, scale bar 3 μm. Inset: scale bar 1 μm. (D) A closer view of (C), scale bar 500 nm.

In the subsequent purification process, SWNT thick silks (1 mm in thickness) were immersed in 3 M H_2SO_4 [or 2 M H_2SO_4/HNO_3 (1:1)] solution at room temperature. Weight loss was about 30% (removing partially amorphous carbon and nanoparticles) after 48 h with little further weight loss after this time. The thick silks were then neutralized in deionized water and resuspended in ethanol. After natural drying, hard thick SWNT films were obtained. A novel fracture was observed in these thick films, as shown in Figure 5. Figure 5a is a low-resolution SEM image of a piece of SWNT thick silk after H_2SO_4-only treatment. The silks after double acid (H_2SO_4 and HNO_3) treatments had similar surface morphology. Many flaws can be seen along the surface with a width of 1 μm to 3 μm. Figure 5b shows the higher resolution SEM image of one typical broken fragment after H_2SO_4 treatment. Inset is a closer view of the parallel arrays of the stretched SWNT bundles bridging the crack. From this image, we can see the pulled SWNT bundles cross over the flaw, showing a good orientation degree just like some relaxed curves.[12] Figure 5c is the SEM image of surface fracture after double-acid treatments. Most SWNT bundles were breaking, generating a series of free-standing SWNT arrays of bundles on the edge of the fracture. The enlarged view of the normally generated high-density SWNT bundles is shown in the inset and Figure 5d, showing good alignments normal to the edge of each crack. The tips of SWNT arrays showed some traces when fractures were made.

Many of the potential applications of single-walled carbon nanotubes (SWNTs) depend on the alignment of the as-grown materials, which is still a big challenge for us.[13] Unfortunately, aligned SWNT arrays could not yet be produced directly with a dense bulk array structure. Some posttreatments have been developed to align SWNTs,[4,14−20] but these posttreatments suffer the constraint that they generate only fiber-like products[4] or film-like materials[16] with discrete morphology. We believe that the formation of well-aligned arrays of SWNT bundles in our SWNT silks profited first from the densely entangled morphology of the raw materials. After acid treatments, the strongly oxidizing acid could react with amorphous carbon, which resulted in the formation of some functional groups on the surface of SWNT bundles, making them coalesce. At the same time, the amorphous carbons were removed effectively and bundles could slide past each other easily. The chemical robustness of SWNTs enabled them survive such long-term exposure to the oxidizing acid. But some defects, which acted as the "yielding points" in SWNT films, were generated in some areas of bundles because of the oxidation of H_2SO_4. In other areas, the residual amorphous carbon welded the SWNT bundles, entangling each other and maintaining the film form. Thus, the thick films were changed from isotropic to anisotropic. In the procedure of natural drying, internal stress was generated because of the different contraction rate at different parts of the heterogeneous film. In addition, the discrepancy of volume change was another origin of the internal stress. Internal stress broke the surface of SWNT films but could not tear them for the limited low value of stress presented in films. When the H_2SO_4/HNO_3 mixture was introduced, stronger oxidation made more defects on the bundles, even breaking them. So the internal stress could split the film and form bulk aligned SWNT bundles. For the purpose of comparison, we also carried out the same procedure using other nonoxidizing acids (such as HCl). The flaws could not be observed in dried materials without the oxidizing acid treatments. The result supported that the dense SWNT raw materials were a unique product and also implied that internal stress played an important role for aligning the SWNT bundles.

In summary, we have modified the conventional arc-discharge method for the synthesis of high-quality SWNT silks using a hollow cathode that can collect SWNTs. Under optimized

conditions, SWNT thin films can be efficiently produced with high purity of over 70%. This is a new kind of SWNT thin silk, which has many potential applications. By applying the Brunauer−Emmett−Teller (BET) method to the adsorption data of N_2 at 77 K on the as-grown SWNTs, we obtain the specific surface area of ~245 m^2/g. The adsorption isotherm was typical Type I due to micropores at the range of $P/P_0 < 0.8$. A substantial increase in the uptake of N_2 occurs at high P/P_0 (>0.8) due to capillary condensation. There is also some hysteresis in the high P/P_0 regime which, due to the intertubular space (aggregated pores formed by the confined space among the isolated bundles), shows Type IV isotherm characteristics associated with capillary condensation in mesopores. The pore size distribution is obtained by the Horvath−Kawazoe (HK) method, showing a major peak around 1.28 nm, corresponding to the average diameter of SWNTs. Due to their high surface area and favorable pore distribution, it is expected that the high purity materials have excellent double-layer capacitance performance.

The macroscopic electrical resistivity of the SWNT silks was also measured on some of the as-grown silks (with thickness from 100 μm to 1 mm) from room temperature to 4.2 K by a four-probe method. Though a high content of metallic SWNTs was present in the silks, macroscopic conducting measurements show that the SWNT silks are semiconductors in the range of 4~300 K for their entangled morphology. So, due to its macroscopic quasi-semiconductivity, electrodes can be deposited on the surface to build field-effect tubes (FETs).

Acknowledgment. The financial support of this work by the State Key Program for Fundament Research of the Ministry of Science and Technology (MOST), China (Grant No. G20000264-04) is acknowledged.

References and Notes

(1) Journet, C.; Maser, W. K.; Bernier, P.; Loiseau, A.; Lamy de la Chapelle, M.; Lefrant, S.; Deniard, P.; Lee, R.; Fischer, J. E. *Nature* **1997**, *388*, 756.

(2) Huang, H.; Kajiura, H.; Tsutsui, S.; Hirano, Y.; Miyakoshi, M.; Yamada, A.; Ata, M. *Chem. Phys. Lett.* **2001**, *343*, 7.

(3) Huczko, A.; Lange, H.; Sioda, M.; Zhu, Y. Q.; Hsu, W. K.; Kroto, H. W.; Walton, D. R. M. *J. Phys. Chem. B* **2002**, *106*, 1534.

(4) Vigolo, B.; Penicaud, A.; Coulon, C.; Sauder, C.; Pailler, R.; Journet, C.; Bernier, P.; Poulin, P. *Science* **2000**, *290*, 1331.

(5) Liu, C.; Cheng, H. M.; Cong, H. T.; Li, F.; Su, G.; Zhou, B. L.; Dresselhaus, M. S. *Adv. Mater.* **2000**, *12*, 1190.

(6) Zhu, H. W.; Xu, C. L.; Wu, D. H.; Wei, B. Q.; Vajtai, R.; Ajayan, P. M. *Science* **2002**, *296*, 884.

(7) Thess, A.; Lee, R.; Nikolaev, P.; Dai, H. J.; Petit, P.; Robert, J.; Xu, C. H.; Lee, Y. H.; Kim, S. G.; Rinzler, A. G.; Colbert, D. T.; Scuseria, G. E.; Tomanek, D.; Fischer, J. E.; Smalley, R. E. *Science* **1996**, *273*, 483.

(8) Rinzler, A. G.; Liu, J.; Dai, H.; Nikolaev, P.; Huffman, C. B.; Rodriguez-Macias, F. J.; Boul, P. J.; Lu, A. H.; Heymann, D.; Colbert, D. T.; Lee, R. S.; Fischer, J. E.; Rao, A. M.; Eklund, P. C.; Smalley, R. E. *Appl. Phys. A* **1998**, *67*, 29.

(9) Kataura, H.; Kumazawa, Y.; Maniwa, Y.; Umezu, I.; Suzuki, S.; Ohtsuka, Y.; Achiba, Y. *Synth. Met.* **1999**, *103*, 2555.

(10) Li, H. D.; Yue, K. T.; Lian, Z. L.; Zhan, Y.; Zhou, L. X.; Zhang, S. L.; Shi, Z. J.; Gu, Z. N.; Liu, B. B.; Yang, R. S.; Yang, H. B.; Zou, G. T.; Zhang, Y.; Iijima, S. *Appl. Phys. Lett.* **2000**, *76*, 2053.

(11) Chiang, I. W.; Brinson, B. E.; Smalley, R. E.; Margrave, J. L.; Hauge, R. H. *J. Phys. Chem. B* **2001**, *105*, 1157.

(12) Ajayan, P. M.; Schadler, L. S.; Giannaris, C.; Rubio, A. *Adv. Mater.* **2000**, *12*, 750.

(13) *Carbon Nanotubes: Synthesis, Structure, Properties and Applications*; Dresselhaus, M. S., Dresselhaus, G., Avouris, Ph., Eds.; Springer: New York, 2001.

(14) Andrews, R.; Jacques, D.; Rao, A. M.; Rantell, T.; Derbyshire, F.; Chen, Y.; Chen, J.; Haddon, R. C. *Appl. Phys. Lett.* **1999**, *75*, 1329.

(15) Gommans, H. H.; Alldredge, J. W.; Tashiro, H.; Park, J.; Magnuson, J.; Rinzler, A. G. *J. Appl. Phys.* **2000**, *88*, 2509.

(16) Haggenmueller, R.; Gommans, H. H.; Rinzler, A. G.; Fischer, J. E.; Winey, K. I. *Chem. Phys. Lett.* **2000**, *330*, 219.

(17) Smith, B. W.; Benes, Z.; Luzzi, D. E.; Fischer, J. E.; Walters, D. A.; Casavant, M. J.; Schmidt, J.; Smalley, R. E. *Appl. Phys. Lett.* **2000**, *77*, 663.

(18) Nagahara, L. A.; Amlani, I.; Lewenstein, J.; Tsui, R. K. *Appl. Phys. Lett.* **2002**, *80*, 3826.

(19) Chen, J.; Weimer, W. A. *J. Am. Chem. Soc.* **2002**, *124*, 759.

(20) Shimoda, H.; Oh, S. J.; Geng, H. Z.; Walker, R. J.; Zhang, X. B.; McNeil, L. E.; Zhou, O. *Adv. Mater.* **2002**, *14*, 899.